Solid state synthesis of Zeolite-Templated Carbons

Thibaud Aumond, Annaig Le Person, Isabelle Batonneau-Gener, Hervé Vezin, Alexander Sachse, Alain Moissette

Solid state synthesis of Zeolite-Templated Carbons

Thibaud Aumond,[a,b] Annaig Le Person,[a] Isabelle Batonneau-Gener,[b] Hervé Vezin,[a] Alexander Sachse,[b] Alain Moissette [a]*

[a]Laboratoire de Spectroscopie pour les Interactions la Réactivité et l'Environnement Université de Lille, UMR CNRS 8516-LASIRE, 59000 Lille (France)
[b]Institut de Chimie des Milieux et Matériaux de Poitiers (IC2MP), Université de Poitiers – UMR 7285 CNRS, UFR SFA, Bat. B27, 4 rue Michel Brunet, TSA 51106, 86073 Poitiers, Cedex 9, France.

Abstract

The first solid state synthesis of Zeolite-Templated Carbons (ZTC) is reported using anthracene as carbon precursor in **FAU** structured zeolite. The evolution of the anthracene molecule upon sublimation inside of the zeolite micropore system and its further condensation into larger polyaromatic species could be followed by DRUV and Raman spectroscopy. The development of the anthracene radical cation through spontaneous charge separation was found to play a fundamental role in the formation of the carbon skeleton. A cyclic radical formation and recombination behavior could be revealed by *in situ* EPR spectroscopy. Textural and chemical characterization of the hybrid (zeolite/ZTC) and of the ZTC upon zeolite removal allowed to conclude that anthracene allows for achieving ZTC materials with transcribed morphological and textural properties of the template zeolite. The impact of the thermal treatment on the ZTC properties was further studied. ZTCs with emerging structural order could be achieved.

I. Introduction

Zeolite Templated Carbons (ZTCs) are carbon-based materials that are generated by the use of sacrificial zeolite templates. This material's family outstands through their unique properties combining electrical conductivity and tailored topology of micropores.[1] Numerous gaseous and liquid carbonaceous precursors have been reported to allow for the synthesis of

ZTCs.[2-4] In the former case, the synthesis is often described as chemical vapor deposition,[5-7] this designation has yet strongly been questioned as the chemical properties of the zeolite strongly impact the nature of the resulting ZTC.[8] Light hydrocarbons, such as acetylene, ethylene or propene, but also methane are frequently used as gaseous carbon precursors.[1] Such small molecules can freely diffuse in 12-ring zeolites (such as those featuring **FAU**, **EMT** or ***BEA** structure) and react in the micropore system to allow for the formation of a negative copy of the zeolite structure, which is recovered as ZTC after zeolite dissolution. Impregnation of the zeolite template with liquid precursors was further proposed and is generally carried out at room temperature (RT).[1] Commonly used liquid precursors in ZTC synthesis contain heteroatoms, and include furfuryl alcohol and glucose both containing oxygen atoms, or acetonitrile and acrylonitrile that feature nitrogen atoms. The use of such liquid precursors has been described to lead to ZTCs of minor structural quality and the subsequent use of a gaseous carbon source is generally advised to generate hybrid zeolite/ZTC featuring high structural packing density. Moreover, solutions, such as pyrene in toluene were used in the quest of synthetizing functional ZTCs.[9] Despite the use of an ample range of carbon precursors, pure solids have to date not been reported as precursors for the generation of ZTCs.

On the other hand, it is well known that certain polyaromatic molecules, such as anthracene or *trans*-stilbene, are able to penetrate into the zeolite microporosity by sublimation and intracrystalline diffusion.[10-14] The incorporation into the zeolite microporosity can spontaneously induce ionization of the aromatic molecule if high confinement and low potential energy of the guest and electron acceptor sites are present.[11] Spontaneous ionization of aromatic molecules leads to the formation of radical cations generating often stable separated charge states which play a key role in the formation of ZTC material.[8]

The sublimation of solid aromatic molecules has so far only been studied from a molecular point of view and using low aromatics/zeolite ratios. In the present contribution we firstly report the synthesis of ZTC using anthracene as solid carbon precursor. The achieved results allow for highlighting the crucial role of spontaneous charge separation of polyaromatic molecules in ZTC synthesis.

II. Experimental

1. Materials

CBV500 (Zeolyst International, Si/Al = 2.6, hereafter named FAU) was calcined at 550 °C under air before use (rate: 1 °C $min^{-1)}$. Anthracene ($C_{14}H_{10}$, Merck-Schuchardt), hydrofluoric acid (Fisher Scientific, 49wt % in water), boric acid (Sigma Aldrich, 99 %), sodium bicarbonate (Sigma Aldrich, 99 %), and N_2 (> 99.995 %, Air Liquide) were used as received.

2. Sample preparation

- *Preparation of the Anth@FAU precursors*

The FAU zeolite samples used in the following experiments were used after a calcination procedure under argon at 500 °C. After calcination, the dehydrated host material was cooled to room temperature. Then, anthracene (Anth) corresponding to 0.33 g Anth per g of FAU (about 20 molecules per Unit Cell) was introduced into the cell under dry argon and the adsorption of Anth in empty FAU takes place by sublimation. Finally, the powder was transferred under dry argon to a quartz glass Suprasil cell for spectral experiments.

- *Hybrids*

Hybrid materials were prepared by heating the precursors Anth@FAU at 700, 800, 900 or 1000 °C during the heat treatment (HT) process. 1 g of precursor was placed in a furnace that was heated at 150 °C under N_2 (150 mL min^{-1}) in order to remove physisorbed water. Then, the precursor was heated at heat treatment temperature for 2 h. After cooling down to room temperature, the hybrid material is recovered and characterized.

- *Zeolite Templated Carbon (ZTC) materials*

Carbon materials were formed for each hybrid material obtained for different heating temperatures after the complete dissolution of the zeolite. 0.5 g of the hybrid compound was transferred to a Teflon beaker and stirred with 5 mL of aqueous HF solution for 4 hours at room temperature. In order to neutralize the fluoride, 30 mL of a saturated aqueous H_3BO_3 solution was added. The mixture was then neutralized through adding 30 mL of a saturated aqueous $NaHCO_3$ solution. After 1 hour of stirring at room temperature, the carbon materials were recovered by filtration and abundantly washed with hot deionized water and thereafter dried at 80 °C for 12 hours.

The hybrid materials and subsequent ZTC materials obtained after activation of the zeolite at 500 °C are referred to as H-TEMP and ZTC-TEMP, respectively, where TEMP is the heat treatment temperature of 700, 800, 900 or 1000 °C.

3. Characterization techniques

- *Diffuse reflectance UV-visible absorption spectroscopy (DRUVv).* Adsorption and diffusion of anthracene into the zeolite materials were followed after mixing Anth with proton-exchanged FAU (Si/Al = 2.6) using a Cary 6000 UV-vis spectrometer. The instrument was equipped with an integrating sphere to study the powdered zeolite samples through diffuse reflectance. DRUVv spectra were plotted as the Kubelka–Munk function.

- *Raman scattering.* Raman analyses of the precursors, hybrids and ZTC were carried out on a LabRam HR-Evolution (Horiba scientific) micro-spectrometer equipped with a 600 lines per mm grating using a 100 × 0.9 NA Olympus objective and a λ_{ex} = 515 nm excitation wavelength (1% laser power). Data processing was performed using LabSpec6 software.

- *EPR.* Continuous-wave electron paramagnetic resonance (CW-EPR) spectra were recorded at room temperature using a Bruker ELEXSYS E500 spectrometer operating at X-band. Microwave power and amplitude modulation were respectively set to 5 mW and 1 G. Quantification of radical content was achieved using the Bruker weak-pitch standard sample (containing 1.09 10^{13} spin g^{-1}). The spin concentration is calculated from the double integration of the first derivative of the EPR signal. Pulsed-EPR experiments were carried out at 5 K using a CoolEdge cryofree cryostat system. 2D Hyperfine Sublevel Correlation (HYSCORE) method was used for detecting ^{1}H, ^{13}C and ^{29}Si nuclei. The following pulse scheme was used $\pi/2-\tau-\pi/2-t_1-\pi-t_2-\pi/2-\tau$ echo and a four-step phase cycling where the echo is measured as a function of t_1 and t_2, with t1 and t_2 being incremented by steps of 16 ns from their initial values. The τ values were chosen from a 3-pulse ESEEM as function of τ. τ values of 136, 164 and 204 ns were used and all these HYSCORE spectra were summed to obtain final spectra.[15]

- *Organic elemental analyses* were carried out using an EA 1112/Flash 2000 Thermo photo flash to determine the composition in carbon, oxygen and hydrogen of the carbonaceous materials.

- *Thermogravimetric analysis (TGA)* was performed using a SDT Q600 from TA Instruments under synthetic air with a flow of 100 mL min^{-1}. The sample was heated up to 900 °C with a ramp of 10 °C min^{-1}. The structural packing density (SPD) corresponds to the amount of carbonaceous species per gram of zeolite ($g_C\ g_{Zeo}^{-1}$).

- *X-Ray powder diffraction (XRD)* patterns were collected using a PANalytical Empyrean X-Ray diffractometer using CuKα radiation (1.54059 Å) from 5 to 50 °2θ ranging.

Nitrogen physisorption was carried out using a Micromeritics 3Flex at -196 °C. Approximately 50 mg of sample was outgassed at 300 °C for 12 h before the measurement. Microporous volumes and specific surface area were calculated through *t*-plot method.

- *Electron microscopy.* Scanning Electron Microscopy (SEM) images were obtained using a JEOL JSM-790CF microscope and Transmission Electron Microscopy (TEM) images using a JEOL 2100 instrument (operating at 200 kV with LaB_6 source and equipped with Gatan Ultra scan camera).

- *Electrical conductivity measurements* were performed using a Solartron 12962A as sample holder in combination with a Solartron SI 1287 electrochemical interface and an SI 1260 impedance/gain-phase analyser.impedance/gain-phase analyser SI 1260

III. Results and discussion

Four distinct steps were identified in the present study. These can be defined as: *i*) preparation and characterization of the precursor at room temperature; allowing to study the initial adsorption and ionization processes of anthracene in the microporosity of FAU structured zeolite, *ii*) demonstration of the involvement of successive intermediate species by applying a moderate and progressive heat treatment, *iii*) characterization of zeolite/ZTC hybrids through high temperature heat treatment, and *iv*) characterization of the ZTC materials obtained upon zeolite.

1. Preparation and characterization of the precursor: first step of ZTC formation

Anth and FAU are white powders before mixing. The mechanical mixing of these two components leads to an immediate color change to light green. As a function of time a color evolution from light to dark green could be observed, indicating progressive diffusion of anthracene into the zeolite porosity.

The CW EPR spectrum recorded after 15 min of mixing features the presence of a hyperfine structure by quadrature detection (**Figure 1**). The resolved structure is characteristic of the Anth radical cation.[16] This signal is centered at a g factor of 2.0043 and is combined with a superimposed broad signal. With time, the hyperfine structure disappears whereas the broad signal still remains. These data confirm the initial formation of the radical cation that rapidly evolves to form subsequent paramagnetic species which can be better characterized by other spectroscopic techniques.

The DRUVv spectra recorded as a function of time show instantaneously the presence of a broad absorption which progressively develops in the 600-900 nm spectral domain, featuring an initial maximum at 710 nm, which can be assigned to the radical cation $Anth^{+\bullet}$, indicating the initial spontaneous ionization of the guest molecule upon adsorption in FAU.[11] The band shifts towards the near infrared with time, between 550 and 1100 nm and maximizes at 760 nm with a shoulder at 695 nm within 4 days after mixing. In addition to this contribution, a band centered at 423 nm corresponding to the protonated form of anthracene ($Anth\text{-}H^{+}$) is also well visible few time after mixing (**Figure 2**).[17]

The spontaneous ionization of Anth occurring concomitantly to the anthracene protonation has been previously reported in protonated Y zeolite and explained by the presence of strong Brønsted and Lewis acid sites.[17] The simultaneous formation of the radical and of the protonated form of Anth are associated with a competitive behavior between the proton affinity (207.0 $kcal.mol^{-1}$) and the ionization potential of anthracene (7.44 eV). It was yet reported that these reaction processes are independent of each other as no interconversion between the radical cation and the protonated species could be evidenced.[17] Note that although the protonated form appeared major immediately after mixing, the spectral signature of this form was fully overlapped after about 8 days (not shown). The spontaneous ionization of the molecules after adsorption depends on the ionization potential of the guest but also on the internal properties of the zeolite host such as the nature of the charge-compensating cation, the acidity, the diameter of the pores inducing a more or less marked confinement effect which will affect the polarization in the porosity at the sorption sites. [18] In particular, confinement within the pores has been identified as a key factor in stabilizing long-lived separated charge states. Indeed, stronger confinement in narrower channels of **MFI** compared to **FAU** structured zeolites allows to induce stabilization of radical cation in high yield over months. By contrast, in the larger cages of **FAU** zeolites, the radical cation is not sufficiently stabilized and evolves after few days to a new species that presents a broad band at 760 nm. This feature might be correlated to the slight red shift and broadening of the radical cation band at 710 nm observed by Hashimoto *et al.* with increasing loading of Anth in NaX attributed to the intermolecular interaction resulting from the close proximity of anthracene molecules in **FAU** supercages exerting attractive forces.[19] However, although strong interaction among molecules is probable, no clear evidence was found allowing to confirm the formation of anthracene dimers, which should result in a red shift of the absorption in the 360-385 nm region with the disappearance of the vibronic band structure.[20-23] Moreover, the

characteristic Raman bands of neutral Anth dimer reported by Ebisuzaki *et al*. are not observed in the present case.[24]

The formation of the dimer radical cation $(Anth)_2^{+\bullet}$, which might be obtained by the association of an $Anth^{+\bullet}$ with a neutral Anth molecule should further be considered. This dimeric species is characterized by a contribution at 680 nm and a second contribution at a wavelength above 900 nm which is attributed to charge delocalization between the molecule and the radical cation due to overlapping π-π orbitals.[25] The observation of a shoulder at about 695 nm and the presence of a broad contribution extending beyond 1100 nm within a few days after spontaneous ionization of Anth could be correlated with the transient formation of such dimeric species. It should furthermore be noted that the ejected electron obtained after ionization is not trapped by another anthracene molecule in the vicinity, which would lead to the formation of an Anth radical anion. Although such a radical anion is assumed to exhibit a band at 730 nm, the latter species is also characterized by intense Raman bands at 608, 1233 and 1359 cm^{-1}, which are not observed in the present study (**Figure 3**).[26-28]
Because of low Anth confinement in FAU supercages and low oxidizing power of the anthracene radical cation (E_{ox} = 1.1 V/SCE), it should further be noted that the new species does not correspond to the charge transfer complex formed by the capture of an electron by the zeolite framework as observed previously with anthracene adsorbed in H-ZSM-5 (**MFI**).[29]

The sorption, ionization and subsequent reactions occurring after mixing of anthracene and FAU were also followed as a function of time by using Raman scattering. The spectra recorded using the 515 nm exciting radiation show the progressive decrease of the Anth contributions, especially the main band at 1401 cm^{-1} which becomes very weak after one week of mixing (**Figure 3**). Parallel to the disappearance of the molecule signature of Anth, the formation of the radical cation is confirmed by the observation of its characteristic bands centered at 1260, 1501 and 1390 cm^{-1} (the latter as a shoulder of the band centered at 1395 cm^{-1}). However, the intensity of these contributions remains very weak and decreases rapidly with time concomitantly with the appearance of new bands at 760, 1183, 1367, 1395, 1555 and 1610 cm^{-1} as observed after four days of contact. For longer times, new bands develop progressively at 1435, 1580 and 1280 cm^{-1} and are clearly observed after three weeks. These bands do not correspond to any known species relative to anthracene. Nevertheless, the bands observed in the 1500-1600 cm^{-1} region probably correspond to C=C stretching characteristic of phenyl ring possibly associated with bigger polyaromatics molecules probably formed by polycondensation of Anth in the cages of FAU initiated by $Anth^{+\bullet}$. Note that these new bands

do not match with the spectral signature of model molecules like pyrene, coronene, pentacene, fluorene, chrysene, **Figure S1**. This spectral evolution is assigned to the first steps of PAH condensation of radical cations within the zeolite since the bands become very broad with time and may correspond to the appearence of the D and G bands classically observed for broader carbonaceous species. Nevertheless, it is interesting to note that the initial ionization of anthracene to form the radical cation $Anth^{+\bullet}$ is followed by different intermediary stages all along the sample evolution with time as shown by the emergence of successive series of Raman bands. For example, the Raman band at 760 cm^{-1} could be ascribed to naphthalene type species (**Figure S1**). This band is formed very early, increases concomitantly to the $Anth^{+\bullet}$ band decrease and begins to decrease after few weeks. As shown in the literature, radical cation $Anth^{+\bullet}$ can evolves spontaneously to smaller and reactive other radical species by hydrogen or acetylene loss such as cyclobutanaphtalene, biphenyl or naphthalene radical cation.[30,31] Even though, these reactions have been only observed in liquid organic polar solvent, it cannot be excluded that they can also take place in zeolite micropores. The powerful electrostatic field in zeolite micropores is known to ionize and stabilize radical species which cannot be spontaneously generated and stabilized in organic solvents. So, these new radical species can certainly recombine or react with other radical species leading to bigger polyaromatic molecules.

2. Synthesis of zeolite/carbon hybrid materials

In order to further study the evolution of Anth, the kinetics of the PAHs growth was accelerated by applying a moderate and progressive heating of the Anth@FAU precursor obtained two days after the mixing of Anth and FAU and monitored as a function of temperature by Raman and EPR spectroscopy.

2.1 Initial stage (heating to 400 °C)

Figure 4 shows the Raman spectra obtained as a function of temperature from room temperature up to 400 °C. It is interesting to note that the spectral evolution of the initial system observed as a function of time (up to three weeks) is identical to that observed under gentle warming at 100 and 150 °C. In particular, the bands at 1183, 1280, 1367, 1395, 1435, 1555, 1580 and around 1610 cm^{-1} are observed up to 150 °C. However, the line centered at 1435 cm^{-1} as well as those at 1580 and 1280 cm^{-1} show a different behavior, their intensity continues to increase for slightly higher temperatures. This result confirms that the evolution

of the system does indeed take place in several steps. For higher temperature (200 to 400 °C), the 1435 cm^{-1} band disappears and only three broad bands at about 1580 cm^{-1}, 1362 cm^{-1} and 1165 cm^{-1} are observed. These latter bands can be assigned as the G (1505-1605 cm^{-1}), D (1330-1400 cm^{-1}) and S (1200 cm^{-1}) bands typically observed in ZTC/zeolite hybrid materials formed using ethylene as carbon source.[8]

The evolution of the radical species was followed *in situ* by CW EPR spectroscopy upon heating to 450 °C. The resolved structure of the $Anth^{\bullet+}$ radical cation (**Figure 1**) was no longer observed after about 30 min at RT, (**Figure 5a**). The Anth@FAU precursor sample was heated applying temperature plateaus with 50 °C increment. For each heating plateau, temperature was kept constant for 2 hours and EPR spectra evolution was monitored. It is interesting to note that the integrated EPR signal exhibits cyclic behavior (**figure 5b)**. At first, the spin concentration increases significantly from 20 to 150 °C and then decreases considerably when the temperature was maintained at 200 °C. A second increase is observed from 250 to 350-400 °C before a slight decrease. Finally, a growth of the integrated signal when the sample was kept at the temperature of 450 °C was observed.

The increase in spin density from 20 to 150 °C reflects the formation of a large number of various radical species as a result of spontaneous ionization of anthracene. The initial spin concentration at 20 °C is very high and cannot only be explained by the anthracene radical cation formation. This species is present in a very low amount indicating that the high spin concentrations might come from other radical aromatic species. The reduction in spin density after the first maximum at 150 °C probably reflects the association of these species to form larger carbon entities by a radical mechanism inducing radical recombination. The subsequent cyclic behavior with successive increases and decreases in spin density is attributed to similar processes towards the formation of increasingly condensed PAH species. One might speculate that the temperature increase induces the required energy allowing for the formation of new radical species, which then at constant temperature lead to further polycondensation process and hence spin recombination. This feature is in agreement with the conspicuous increase of the ionization yield observed when the activation temperature increases as reported after sorption of biphenyl in H-ZSM-5 zeolite.[32] In addition, the shape of the single line centered at a g factor of 2.0043 evolves from a Gaussian to Lorentzian type at 20 °C and then to a stretch Lorentzian type after heating to 450 °C concomitantly to a broadening of the bandwidth with the temperature increase. It is worth noting that the linewidth of the EPR signal is influenced

by the clustering of the spins and that amorphous carbon-based compounds classically display narrow Lorentzian lines.[33]

These characteristics highlight the involvement of different radical species probably formed during the successive steps of the temperature rise in the growth and condensation of carbonaceous species in the zeolite micropores. It is to note that such increase in the CW EPR signal bandwidth was already reported to be correlated with an increase in the degree of connectivity of sp^2 in carbon films [34] and upon formation of anthracene coke from stacking and condensation of anthracene molecules heated at various temperatures.[35] This behavior is thus in agreement with the evolution of the carbonaceous molecules from clustered moieties toward a homogeneous spin system, as previously observed in the ZTC formation in beta zeolite using ethylene.[8]

It is interesting to note that the Raman spectra recorded at 200 and 400 °C during the temperature ramp followed by EPR show analogous behavior to that reported above in **figure 4**. This correlation between EPR and Raman data confirms the formation of various radical species and demonstrates undoubtedly their involvement in the early stages of the condensation of carbonaceous molecules related to the growth and condensation process after the $Anth^{\bullet+}$ disappearance.

To get further information on the nature and distribution of the radical species, pulsed EPR analyses were carried out by conducting 2D hyperfine sublevel correlation experiments (2D-HYSCORE). This technique allows to evidence the couplings through hyperfine interactions between unpaired electron spins and various nuclei such as ^{1}H, ^{13}C and ^{29}Si located in the vicinity of the single electrons.

In **Figure 6a**, two cross peaks ridges are observed at 14.5 MHz corresponding to the Larmor frequency of ^{1}H. The coordinates of the first cross peaks pair centered at the proton nuclear frequency are (10, 20; 20, 10) MHz while the other pair of cross peaks exhibits coordinates at (5, 24; 24, 5) MHz. These features indicate the presence of at least two types of H in the sample and suggest that successive radical types are probably formed consecutively to the process of spontaneous ionization. Based on what is known from the spectral signature of the anthracene radical cation stabilized in the ZSM-5 zeolite, the ^{1}H-crossed peaks ridges at (5, 24; 24, 5) MHz could include the contributions from the radical cation while the (10, 20; 20, 10) MHz peaks can probably be attributed to polyaromatic radical species.[36] In addition, the 2D-HYSCORE pattern displays also cross peaks ridges with coordinates at (1, 6; 6, 1) MHz

centered at 3.7 MHz corresponding to the Larmor frequency of ^{13}C that is attributed to the most coupled ^{13}C with A_{max} = 5 MHz. It is interesting to note that a coupling of 2.3 MHz is also measured for the ^{13}C furthest from the unpaired electrons.

The $^{13}C/^{1}H$ ratio for the Anth@FAU precursor before the temperature rise is found to be 0.14. It should be noted that a signal is further observed at 2.9 MHz corresponding to the Larmor frequency of ^{29}Si from zeolite structure, yet no structural information could be deduced from this data. The 2D-HYSCORE pattern recorded at 5 K after heating the sample at 450 °C is presented in **Figure 6b**. The ^{1}H hyperfine signal shows only one cross peaks ridge with coordinates at (10, 20; 20, 10) MHz centered at 14.5 MHz with a dipolar contribution that can be measured from the vertical shift at 2.3 MHz corresponding to a mean distance between electron/^{1}H of 0.32 nm. This value, which is close to that of the kinetic diameter of the benzene ring, indicates that the electron is located on the aromatic rings at the edges of the large aromatic carbon system. Furthermore, note that the cross-peaks at (5, 24; 24, 5) MHz attributed to the radical cation of anthracene are no longer observed due to the formation of more complex polycondensed aromatic species. The ^{13}C hyperfine signal centered at 3.7 MHz observed for the sample after heating at 450 °C is broader and more intense than that observed for the sample before heating. The $^{13}C/^{1}H$ signal intensity ratio equals to 0.28 and is hence twice as high as that obtained for the sample before heating. The increase of the HYSCORE $^{13}C/^{1}H$ ratio may be correlated to the increase of the number of carbon atoms involved in the π system and therefore confirms the increase of the condensation degree of the carbonaceous system within the zeolite microporosity.[37] This result further implies that H_2 might be released during the heating of the sample. It is to note that the H_2 production has previously been observed in classical ZTC synthesis using ethylene as carbon precursor.[8]

2.2 High temperature treatment

As we have shown in our previous work,[8] high temperature treatments (700 -1000 °C) improve significantly the quality of the final ZTC since it enhances the aromatic polycondensation.

2.2.1 Characterization of hybrid materials

Under inert gas, the precursors were heated to temperatures of 700, 800, 900 and 1000 °C for two hours to form four hybrids and then four ZTCs upon zeolite dissolution.

The TGA curve of Anth@FAU precursor before heat treatment exhibits 2 mass losses centred at around 250 and 550 °C that can respectively be attributed to Anth that did not react (**Figure S2**) and polycondensed compound. On the other hand, the heat treatment allows the complete reaction of the Anth since no mass loss is present at 250 °C even for the lowest heat treatment temperature (figure 7b). The unique mass loss contribution is shifted to higher temperatures with the heat treatment temperatures and raises 650 °C for the hybrid treated at 1000 °C (**Figure 7b**). Thus, the carbonization yield of anthracene can be considered equal to 100 % since no weight loss corresponding to anthracene (around 250 °C) is visible in the TGA of hybrid materials after heat treatment, no matter the temperature. Structural packing density (SPD) in these hybrid compounds decreases from 0.26 to 0.21 g_C/g_{Zeo} for H-700 to H-1000, respectively (**figure 7c).** The decrease in SPD can be explained by a higher degree of condensation of the carbonaceous compounds with increasing temperature, implying hence a stronger dehydrogenation. It is worth noting that these SPD values are lower than those obtained for hybrids formed using ethylene as carbon precursor in **FAU** (around 0.35 g_C/g_{Zeo}). The reduced SPD using anthracene might be related to the size and rigidity of the bulky molecule compared to ethylene.[38] This finding hence indicates a less effective filling of the micropore space of the zeolite by the carbonaceous network formed from anthracene.

The X-ray diffraction patterns indicate stability of the **FAU** structure during thermal treatment, except for the sample prepared at 1000 °C (**figure 7c**). The XRD powder patterns collected for the hybrid materials obtained after high temperature treatments at 700 and 800 °C are very similar to that of parent FAU although a slight shift towards higher 2 theta values is observed, indicating reduction of the cell parameters (24.42 nm for FAU, 24.44 nm for H-700 and 24.31 nm for H-800) and hence unit cell compression during heat treatment. When the heat treatment is carried out at 900 °C, the reduction of the cell parameter is confirmed (23.99 nm) and a slight broadening of XRD peaks is further observed suggesting a decrease of the crystalline domains. Concerning the hybrid compound H-1000, the zeolite XRD peaks are no longer observed and a broad reflection centered at 24° 2θ indicates the amorphization of the zeolite phase. Despite, an intense peak is observed at 2θ = 6.88° which could correspond to the (111) peak of the zeolite, preserved by the presence of carbon in the supercages. It is important to note that a heat treatment at 1000 °C of the zeolite alone leads to a partial amorphization of the zeolite, yet no apparition of a peak at 2θ = 6.88° could be observed in

the XRD pattern (**Figure S3**), which allows to exclude a possible phase transition of the zeolite alone at this temperature.

The Raman spectra of the hybrid materials show two main contributions centered at about 1595 cm^{-1} and 1370 cm^{-1} and a third weaker band around 1200 cm^{-1}(**figure 8a**). To evaluate the carbonaceous fraction within the zeolite porous material, spectral fitting was performed in the 950-1800 cm^{-1} range by using Gaussian, Lorentzian functions or a mixture of both (**figure S4**). Deconvolution was very satisfying using four contributions corresponding to the spectral domain 1590-1600 cm^{-1} associated with the G band for sp^2 carbons, 1510-1535 cm^{-1} related to an intermediate structure between sp^2 carbon and amorphous structure (band R1), 1350-1385 cm^{-1} for the D band of defect carbon or cyclic carbon species and 1195-1215 cm^{-1} also associated to amorphous carbon (band R2). From the area of the G and D bands determined by deconvolution, the evolution of the ratio of the D and G band areas (A_D/A_G) as a function of the heat treatment temperature clearly shows that the defect content is doubled when increasing the temperature from 700 to 1000 °C (**figure 8b**).

Furthermore, a temperature dependency of the G-band position can be observed, which red shifts from 1600 to 1590 cm^{-1} for 700 to 1000 °C, respectively (**figure 9**). This shift can be attributed to a greater delocalization of π-electrons, which hence indicates favored condensation of the carbon skeleton through applying higher temperatures of heat treatment. This confirms the observation of reduced SPD of hybrids prepared at higher temperatures. Moreover a shift of the D-band position could be evidenced from 1382 to 1351 cm^{-1} for 700 and 1000 °C, respectively, which further suggests an increase of the size of the polyaromatic skeleton.[39]

2.2 Characterization of Zeolite-Templated Carbons

After dissolution of the zeolite, the obtained carbon compounds feature a morphology similar to that of the template FAU zeolite (**Figure 10 and Figure S5**). Observation of the SEM images allows to deduce 0.5-1 µm bipyramidal particles shape, which feature the transcription of the steamed mesoporosity present on the template FAU zeolite. The surface of the carbon particles achieved at 700 °C is not smooth and presents defects. This is no longer the case for samples achieved at higher temperatures. Concerning the sample ZTC-1000, despite the

amorphization of the zeolite during the heat treatment, the resulting ZTC still presents perfect morphology replica of the template zeolite.

The transcription of the textural properties to the ZTC-900 was further studied by TEM (**Figure ~~S6~~ 11**). The presence of structured micropores and larger mesopores can be unambiguously assessed, which directly result from zeolite micropore templating and transcription of steamed mesoporosity present in the template zeolite.

The textural properties of the ZTCs were further studied by nitrogen physisorption at 77 K (**Figure 12a**) which all feature very similar shapes compared to the template zeolite.

The ZTC-700 features the lowest micropore volume, which amounts to 0.56 cm^3 g^{-1} (**figure 12b**). The micropore volume increases for the sample ZTC-800 to 0.82 cm^3 g^{-1} and remains constant thereafter with increasing temperature. Except for ZTC-700, the carbon samples present very similar textural properties. Zeolite amorphization at 1000 °C impacts negligibly the micropore volume of the resulting ZTC which equals 0.81 cm^3 g^{-1}. Furthermore, the surface area and the pore size distributions measured for all the ZTCs achieved are given in table S1.

It is important to note that independently of the applied temperature, the desorption branch of the isotherm never loops the adsorption branch for relative pressures of 0.43, indicating a flexible, weakly structured material. The latter phenomenon slightly reduces with increasing temperature indicating that higher temperatures allow for increasing carbon skeleton condensation. This result confirms what was previously deduced from the evolution of the SPD in hybrid materials.

Likewise, the evolution of the C/H ratio suggests increasing condensation of the carbon skeleton with rising temperature of the heat treatment (**Figure 13a**). The electrical conductivity of the carbonaceous materials follows exactly the same trend as the C/H ratio and its value increases as a function of the heat treatment temperature (**Figure 13b**). The overall low electrical conductivity observed for the ZTCs further indicates that only partial carbon skeleton condensation occurred in the confined spaces of the template zeolite micropores.[8]

The XRD patterns of ZTCs allow for deducing a larger peak centered at 6.5° 2θ for materials achieved at higher than 700 °C (**Figure 14**). The presence of this reflection is typical for ZTCs achieved using **FAU** structured zeolites as template and is due to the transcription of the

(111) reflection. The rather low intensity of this reflection indicates the presence of an emerging long-range order, probably through incomplete condensation of the carbon skeleton. Even if the filling takes place by polycondensation of the anthracene molecules, the structural order remains low and the average SPD values are close to a carbon network that is certainly too flexible and can partially collapse when the zeolite structure is destroyed. Furthermore, it should be noted that only the ZTCs obtained at 700 and 1000 °C show broad peaks of low intensity corresponding to the (002) reflection typical of stacked carbon. The absence of this reflection at 800 and 900 °C is further evidence of the rather high quality of the ZTCs obtained at these temperatures (**Figure S6**).

The Raman spectra of the ZTC materials present the same patterns with two main contributions centered at about 1595 and 1370 cm^{-1} and a third weaker band around 1200 cm^{-1} (**Figure S7**). The spectra could be perfectly fitted in the 950-1800 cm^{-1} range using six contributions centered at about 1172, 1240, 1360 (D-band), 1520, 1595 (G-band) and 1653 cm^{-1}. The intensity and area ratios of the G-band to the D-band remain almost constant over the temperature range studied, indicating that the ZTCs from the hybrids all have an identical vibrational signature regardless of the heating temperature (**figure S8**). The Raman spectra show that the D and G bands observed for these ZTCs have become thinner than for the hybrids. This suggests that the hydrofluoric acid treatment removes turbostratic carbons deposed on the outer surface of the zeolite.

4. Conclusion

For the first time, the use of a solid carbon precursor was used for the synthesis of ZTCs. The filling of the zeolite microporosity was achieved by the sublimation of anthracene, which rapidly undergoes charge separation and induces diffusion of radicals within the microporosity. The presence of radicals plays a crucial role in the formation of the condensed carbon skeleton. The growth of the carbon skeleton was found to follow a cyclic behavior in which radical generation and recombination occur. Independently of the applied temperature, the ZTCs present similar morphological, textural and structural properties. The use of high temperatures seems to favor the condensation of the carbon skeleton in the zeolite porosity. Compared to ethylene as carbon source, the larger kinetic diameter and sterical constraints of the anthracene molecule with respect to the micropore size is an important drawback. The

anthracene density in the internal volume of the zeolite is quite low. A more flexible and thin carbon network is formed in zeolite micropores and probably some part collapses after zeolite framework elimination leading to a less ordered and conductive ZTC than those formed using ethylene as carbon source. Although only a weak structural long-range order was observed for ZTCs using Anth as carbon source, this new synthesis approach by sublimation of solid carbon sources opens a new way in ZTC synthesis and is easy to set up. However, the solid carbon source should be carefully chosen. More flexible and reactive carbon source could give better results.

Acknowledgments

The authors acknowledge financial support from the European Union (ERDF) and Région Nouvelle Aquitaine. The authors acknowledge the Characterization platform of the Institute Michel-Eugène Chevreul (CNRS FR2638, LASIRE, University of Lille) for the Raman facilities and support.

References

(1) Nishihara, H.; Kyotani, T. Zeolite-Templated Carbons – Three-dimensional Microporous Graphene Frameworks. *Chem. Commun.* **2018**, *54*, 5648-5673.

(2) Yang, Z.; Xia, Y.; Sun, X.; Mokaya, R. Preparation and Hydrogen Storage Properties of Zeolite-Templated Carbon Materials Nanocast via Chemical Vapor Deposition: Effect of the Zeolite Template and Nitrogen Doping. *J. Phys. Chem. B* **2006**, *110*, 18424-18431.

(3) Hou, P. X.; Yamazaki, T.; Orikasa, H.; Kyotani, T. An Easy Method for the Synthesis of Ordered Microporous Carbons by the Template Technique *Carbon* **2005**, *43*, 2624-2627.

(4) Kyotani, T.; Nagai, T.; Inoue, S.; Tomita, A. Formation of New Type of Porous Carbon by Carbonization in Zeolite Nanochannels. *Chem. Mater.* **1997**, *9*, 609-615.

(5) Miao, J.; Lang, Z.; Xue, T.; Li, Y.; Li, Y.; Cheng, J.; Zhang, H.; Tang, Z. Revival of Zeolite-Templated Nanocarbon Materials: Recent Advances in Energy Storage and Conversion. *Adv. Sci.* **2020**, 2001335.

(6) Nishihara, H.; Imai, K.; Itoi, H.; Nomura, K.; Takai, K.; Kyotani, T. Formation Mechanism of Zeolite-Templated Carbons. *TANSO* **2017**, *280*, 169-174.

(7) Braun, E.; Lee, Y.; Moosavi, S. M.; Barthel, S.; Mercado, R.; Baburin, I. A.; Proserpio, D. M.; Smit, B. Generating Carbon Schwarzites via Zeolite-Templating. *Proc. Natl. Acad. Sci. Unit. States Am.*, **2018,** *115*, E8116-E8124.

(8) Aumond, T.; Batonneau-Gener, I. ; Pouilloux, Y.; Pinard, L.; Wisser, D.; Moreau, M.; Vezin, H.; Moissette, A.; Sachse, A. How do Zeolite-Templated Carbons Grow? *Materials Today Chemistry* **2022**, *26*, 101053.

(9) Meyers, C. J.; Shah, S. D.; Patel, S. C.; Sneeringer, R. M.; Bessel, C. A.; Dollahon, N. R.; Leising, R.A.; Takeuchi, E. S. Templated Synthesis of Carbon Materials from Zeolites (Y, Beta, and ZSM-5) and a Montmorillonite Clay (K10): Physical and Electrochemical Characterization. *J. Phys. Chem. B* **2001**, *105*, 2143-2152.

(10) Márquez, F.; García, H.; Palomares, E.; Fernández, L.; Corma, A. Spectroscopic Evidence in Support of the Molecular Orbital Confinement Concept: Case of Anthracene Incorporated in Zeolites. *J. Am. Chem. Soc.* **2000**, *122*, 6520-6521.

(11) Moissette, A. ; Marquis, S.; Gener, I. ; Brémard, C. Sorption of Anthracene, Phenanthrene and 9,10-Dimethylanthracene on Activated Acid HZSM-5 Zeolite. Effect of Sorbate Size on Spontaneous Ionization Yield. *Phys. Chem. Chem. Phys.* **2002**, *4*, 5690-5696.

(12) Hureau, M.; Moissette, A.; Marquis, S. ; Bremard, C. ; Vezin, H. Incorporation and electron transfer of anthracene in pores of ZSM-5 zeolites. Effect of Brønsted acid site density. *Phys. Chem. Chem. Phys.* **2009**, *11*, 6299-6307.

(13) Marquis, S.; Moissette, A. ; Brémard, C. Spectroscopic Evidence of the Incorporation of Anthracene into Medium Pores MnZSM-5 Zeolites (M= Na+, K+, Rb+, Cs+). Effect of the Confinement on the Recombination Rate of Photoinduced Radical cation-Electron Pair. *Chem. Phys. Chem.* **2006**, *7*, 1525-1534.

(14) Hureau, M. ; Moissette, A. ; Vezin, H. ; Brémard, C. ; Orio, M. Influence of Confinement Effect on Electron Transfers Induced by t-Stilbene Sorption in Medium Pore Acidic Zeolites. *J. Phys. Chem. C* **2012**, *116*, 1812–1825.

(15) Tayeb, K.B.; Hamieh, S.; Canaff, C.; Nguyen, H.; Vezin, H.; Pinard, L. The radical internal coke structure as a fingerprint of the zeolite framework, *Microporous Mesoporous Mater.* **2019**, *289*, 109617.

(16) Caldararu, H.; Caragheorgheopol, A.; Russu, R. The Strength of One-electron Acceptor Sites of some X and Y Zeolites: an ESR Study. *Colloids Surfaces A: Physicochem. Eng. Aspects* **1993**, *72*, 37-41.

(17) Liu, X.; Iu, K. K.; Thomas, J. K.; He H.; Klinowski, J. Spectroscopic Studies of Protonated Aromatic Species and Radical Cations in H+-Zeolites. *J. Am. Chem. Soc*. **1994**, *116*, 11811–11818.

(18) Moissette, A.: Hureau, M.; Vezin, H.; Lobo, R. Electron transfers under confinement in channel type zeolites in "Chemistry of Silica and Zeolite-based Materials: Synthesis, Characterization and Applications", Abderrazzak Douhal and Masakazu Anpo (Edts.), Elsevier, **2019,** 249-271, ISBN:9780128178133.

(19) Hashimoto, S.; Mutoh, T.; Fukumura, H.; Masuhara, H. Diffuse Reflectance Laser Photolytic Studies of Naphthalene, Biphenyl and some Aromatic Hydrocarbons Adsorbed in the Cavities of Faujasitic Zeolites. *J. Chem. Soc., Faraday Trans.* **1996**, *92*, 3653-3660.

(20) Kwon, O-H.; Yu, H.; Jang, D-J. Formation Mechanism of Anthracene Dimers and Excimers in NaY Zeolitic Nanocavities. *J. Phys. Chem. B* **2004**, *108*, 3970-3974.

(21) Matsuoka, T.; Kosugi, K.; Hino, K.; Nishiguchi, M.; Ohashi, K.; Nishi, N.; Sekiya, H. Electronic Spectra of Jet-Cooled Anthracene Dimer: Evidence of Two Isomers in the Electronic Ground State. *J. Phys. Chem. A* **1998**, *102*, 7598-7602.

(22) Chandross, E. A.; Ferguson, J.; McRae, E. G. Absorption and Emission Spectra of Anthracene Dimers. *J. Chem. Phys.* **1966**, *45*, 3546-3553.

(23) Hashimoto, S.; Hagiri, M.; Matsubara N.; Tobita, S. Photophysical Studies of Neutral Aromatic Species Confined in Zeolite L: Comparison with Cationic Dyes. *Phys. Chem. Chem. Phys.* **2001**, *3*, 5043–5051.

(24) Ebisuzaki, Y.; Taylor, T.J.; Woo, J.T.; Nicol, M. Raman and Luminescence Spectra of Dianthracene at High Pressures. *J. Chem. Soc., Faraday Trans 2* **1977**, *73*, 253-264.

(25) Kochi, J.K.; Rathore, R.; Le Maguères, P. Stable Dimeric Aromatic Cation−Radicals. Structural and Spectral Characterization of Through-Space Charge Delocalization. *J. Org. Chem.* **2000**, *65*, 6826-6836.

(26) Takahashi, C.; Maeda, S. Raman Spectra of Anthracene Negative Ions in Tetrahydrofuran Solution. *Chem Phys. Lett.* **1973**, *22*, 364-367.

(27) Juneau, A.; Frenette, M. Raman Spectra of Persistent Radical Anions from Benzophenone, Fluorenone, 2,2′-Bipyridyl, 4,4′-Di-tert-butyl-2,2′-dipyridyl, and Anthracene: Excellent Agreement between DFT and Experiment for Highly Delocalized Radical Systems. *J. Phys. Chem. B* **2021**, *125*, 1595-1603.

(28) Pedersen, S.U.; Christensen, T.B.; Thomasen, T.; Daasbjerg, K. New Methods for the Accurate Determination of Extinction and Diffusion Coefficients of Aromatic and Heteroaromatic Radical Anions in N,N-Dimethylformamide. *J. Electroanal. Chem.* **1998**, *454*, 123-143.

(29) Vezin, H.; Moissette, A.; Brémard, C. Temperature-Dependent Interconversion of an Anthracene Radical Cation/Electron Moiety to an Electron –Hole Pair in the Pores of Al-ZSM-5 Zeolites. *Angew. Chem. Int. Ed.* **2003**, *42*, 5587-5591.

(30) Ling. Y.; Martin, J. M. L.; Lifshitz, C. Energetics of Acetylene Loss from C14H10•+ Cations: A Density Functional Calculation. *J. Phys. Chem. A* **1997**, *101*, 219-226.

(31) West, B.; Sit, A.; Mohamed, S.; Joblin, C.; Blanchet, V.; Bodi, A.; Mayer, P. M. Dissociation of the Anthracene Radical Cation: A Comparative Look at iPEPICO and Collision-Induced Dissociation Mass Spectrometry Results. *J. Phys. Chem. A* **2014**, *118*, 9870-9878.

(32) Marquis, S.; Moissette, A.; Vezin, H.; Bremard, C., Spontaneous Ionization of Polyaromatics by Sorption in ZSM-5 zeolites. *C. R. Chimie* **2005**, *8*, 419-440.

(33) Barklie, R.C. Characterisation of Defects in Amorphous Carbon by Electron Paramagnetic Resonance. *Diamond and related Materials* **2003**, *12*, 1427-1434.

(34) Tabbal, M.; Christidis, T.; Isber, S. Correlation between the *sp*2-phase Nanostructure and the Physical Properties of Unhydrogenated Carbon Nitride. *J. Appl. Phys.* **2005**, *98*, 044310.

(35) Simon, C.; Estrade, H.; Tchoubar, D.; Conard, J. Etude des Semi-cokes d'Anthracene: Relation entre leurs Proprietes Structurales et Electroniques. *Carbon* **1977**, *15*, 211-218.

(36) Marquis, S.; Moissette, A.; Vezin, H.; Bremard, C. Long-Lived Radical Cation-Electron Pairs Generated by Anthracene Sorption in Non Brønsted Acidic Zeolites. J. *Phys. Chem. B Letters* **2005**, *109*, 3723-3726.

(37) Ikoma, T.; Ito, O.; Tero-Kubota S.; Akiyama, K. HYSCORE Study on Coal Radicals. *Energy & Fuels* **1998**, *12*, 1363-1368.

(38) Aumond, T.; Rousseau, J.; Pouilloux, Y.; Pinard, L.; Sachse, A. Synthesis of Hierarchical Zeolite Templated Carbons. *Carbon Trends* **2021**, *2*, 100014.

(39) Smith, M. W.; Dallmeyer, I.; Johnson, T. J.; Brauer, C. S.; McEwen, J.-S.; Esoinal, J. F.; Garcia-Perez, M. Structural analysis of char by Raman spectroscopy: Improving band

assignments through computational calculations from first principles. *Carbon* **2016**, *100*, 678-692.

Figure caption

Figure 1. *CW EPR spectrum recorded 15 minutes after the mixing the Anth and FAU. The spectrum has been recorded using quadrature detection*

Figure 2. *DRUVv spectra recorded as a function of time from 10 minutes to 4 days after mixing Anth and FAU.*

Figure 3. *Raman spectra obtained after mixing Anth and FAU. The spectra of pure Anth and* $Anth^{+\bullet}$ *are given for comparison. Red arrows indicate weak* $Anth^{+\bullet}$ *contributions.*

Figure 4: *Raman spectra recorded as a function of temperature for Anth@FAU precursor after mixing Anth and FAU.*

Figure 5*: a) CW EPR spectra recorded for the Anth@FAU precursor before and after the temperature rise from 20 °C (RT, black signal) to 450 °C (red signal).*
b) EPR integrated signal recorded as a function of temperature by applying a temperature rise from room temperature (20°C) to 450 °C.

Figure 6. *2D-HYSCORE spectra summed over the 3 τ values of the Anth@FAU precursors before (a) and after (b) the temperature rise at 450 °C. The spectra were recorded at 5 K.*

Figure 7: *a) TGA mass loss curves, b) SPD and c) X-ray diffraction patterns of hybrids obtained under different heat treatments*

Figure 8: *a) Raman spectra obtained for hybrid compounds after heat treatment of Anth@FAU precursor at 700, 800, 900, and 1000 °C. b) Evolution of the* A_D/A_G *ratio as a function of the heat treatment temperature*

Figure 9: *Raman shift of the G and D band positions as a function of the heat treatment temperature for the hybrid materials obtained at 700, 800, 900, 1000 °C.*

Figure 10*: SEM images of ZTC achieved at 700, 800, 900 and 1000 °C.*

Figure 11: *TEM images of template FAU (a) and ZTC-900 (b).*

Figure 12*: a) N_2 physisorption isotherms and b) microporous volumes of ZTC carbonaceous materials obtained by different thermal treatments*

Figure 13: *a) Composition of carbonaceous materials, and b) Electrical conductivity of these materials normalized by the conductivity of graphite.*

Figure 14: *X-ray diffraction patterns of ZTCs obtained after different heat treatments.*

Figure 1

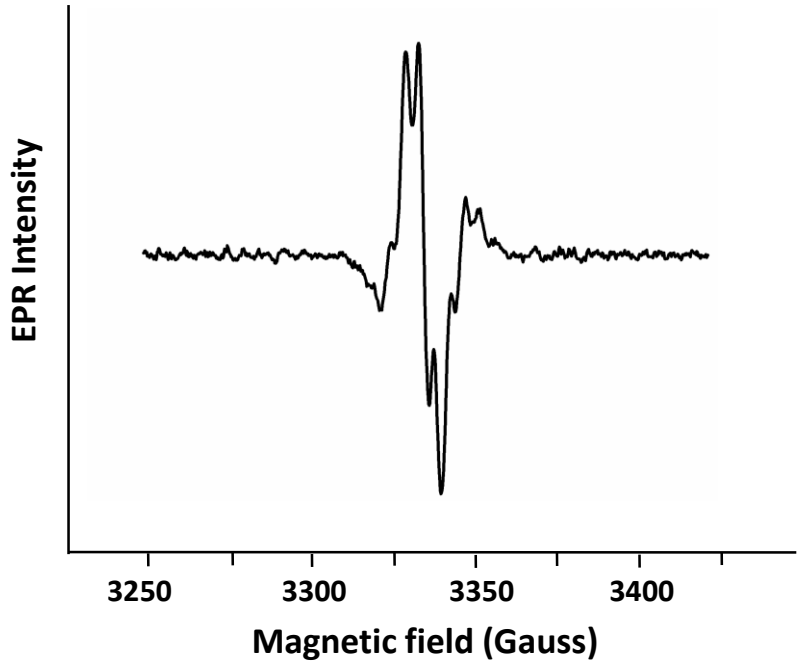

Figure 2

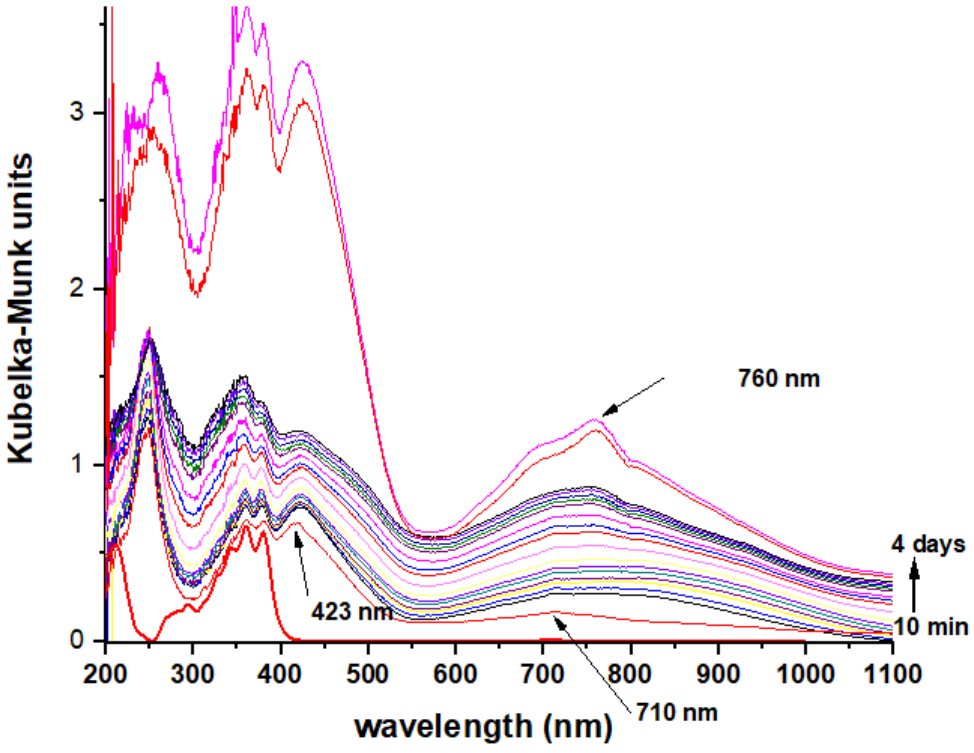

Figure 3

Figure 4

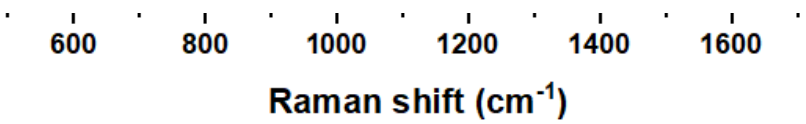

Figure 5

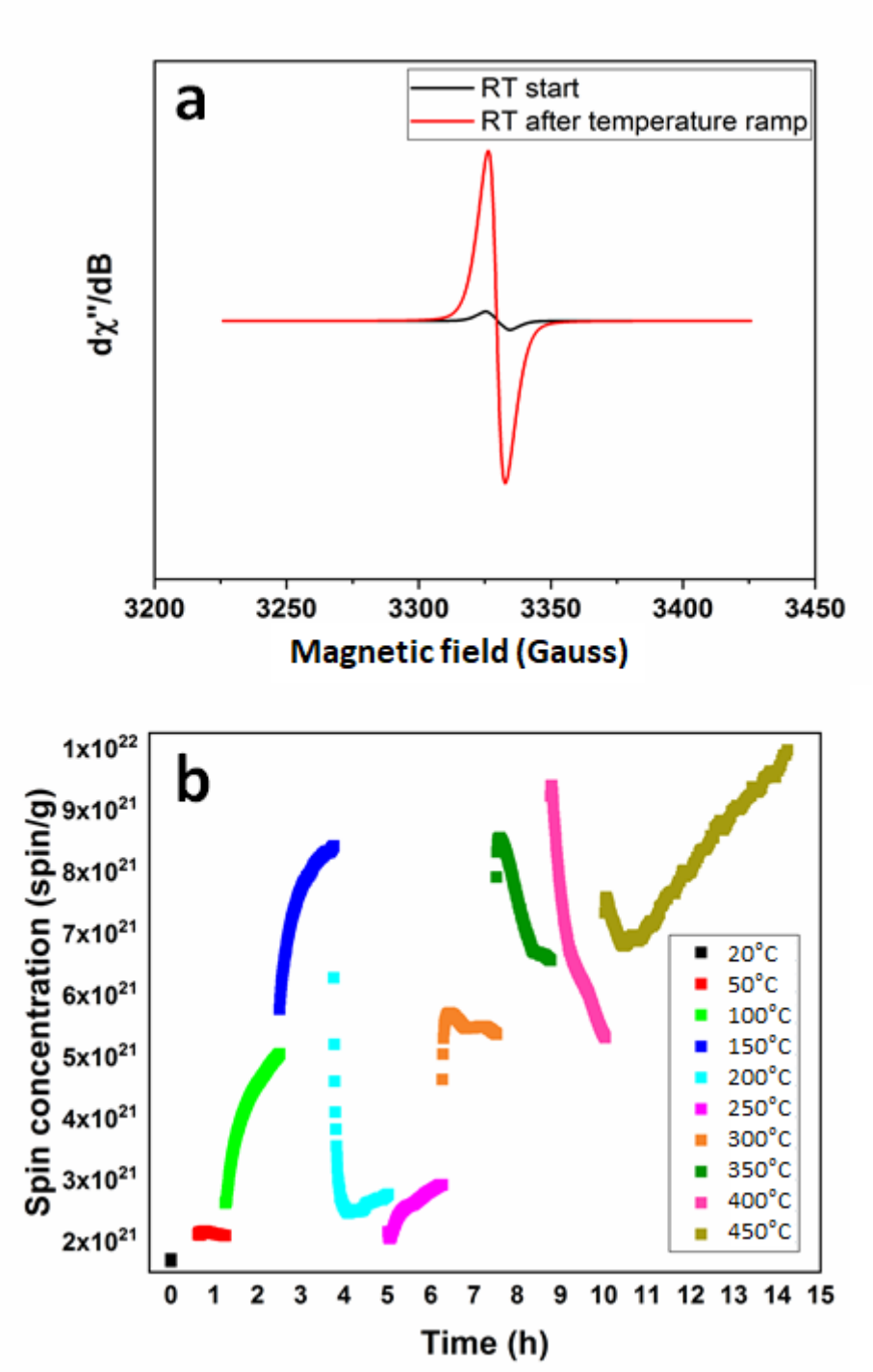
a
RT start
RT after temperature ramp
dχ''/dB
3200
3250
3300
3350
3400
3450
Magnetic field (Gauss)
b
Spin concentration (spin/g)
1x10^22
9x10^21
8x10^21
7x10^21
6x10^21
5x10^21
4x10^21
3x10^21
2x10^21
0 1 2 3 4 5 6 7 8 9 10 11 12 13 14 15
Time (h)
20°C
50°C
100°C
150°C
200°C
250°C
300°C
350°C
400°C
450°C

Figure 6

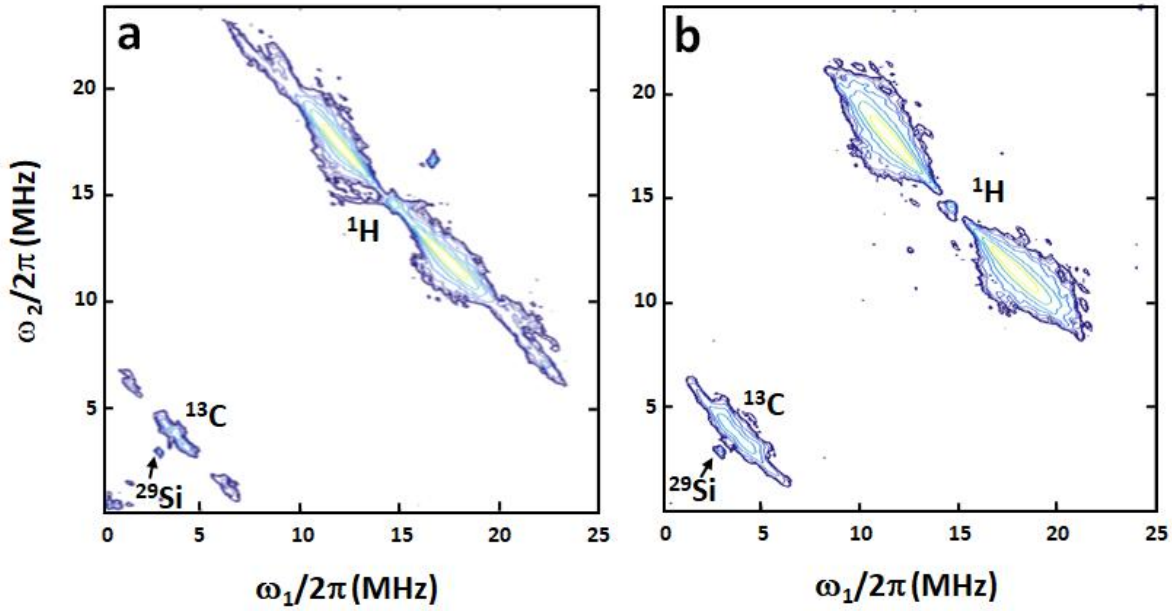

Figure 7

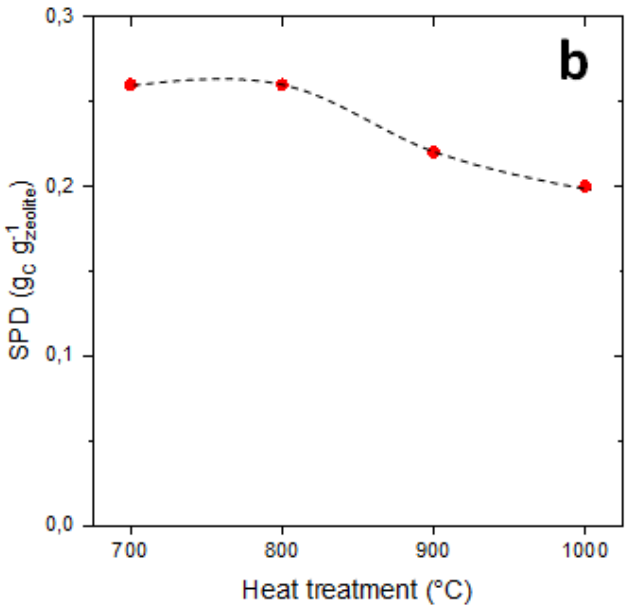
b
0,3
0,2
0,1
0,0
SPD (gC gzeolite-1)
700
800
900
1000
Heat treatment (°C)

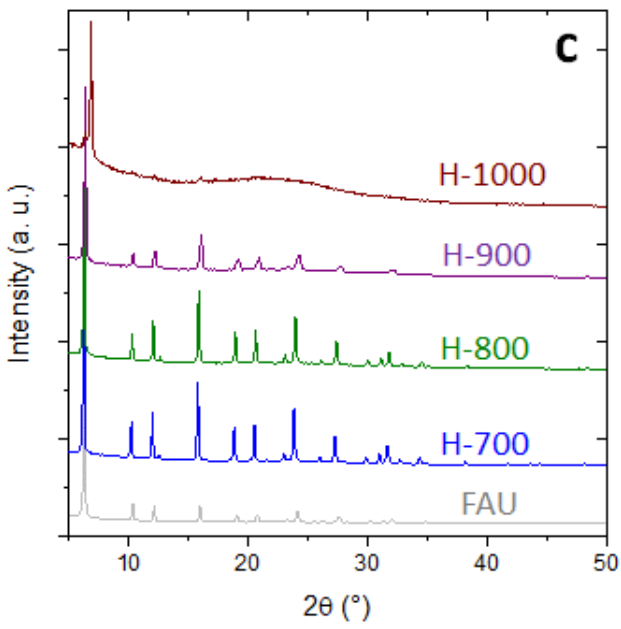
c
H-1000
H-900
H-800
H-700
FAU
Intensity (a. u.)
10
20
30
40
50
2θ (°)

Figure 8

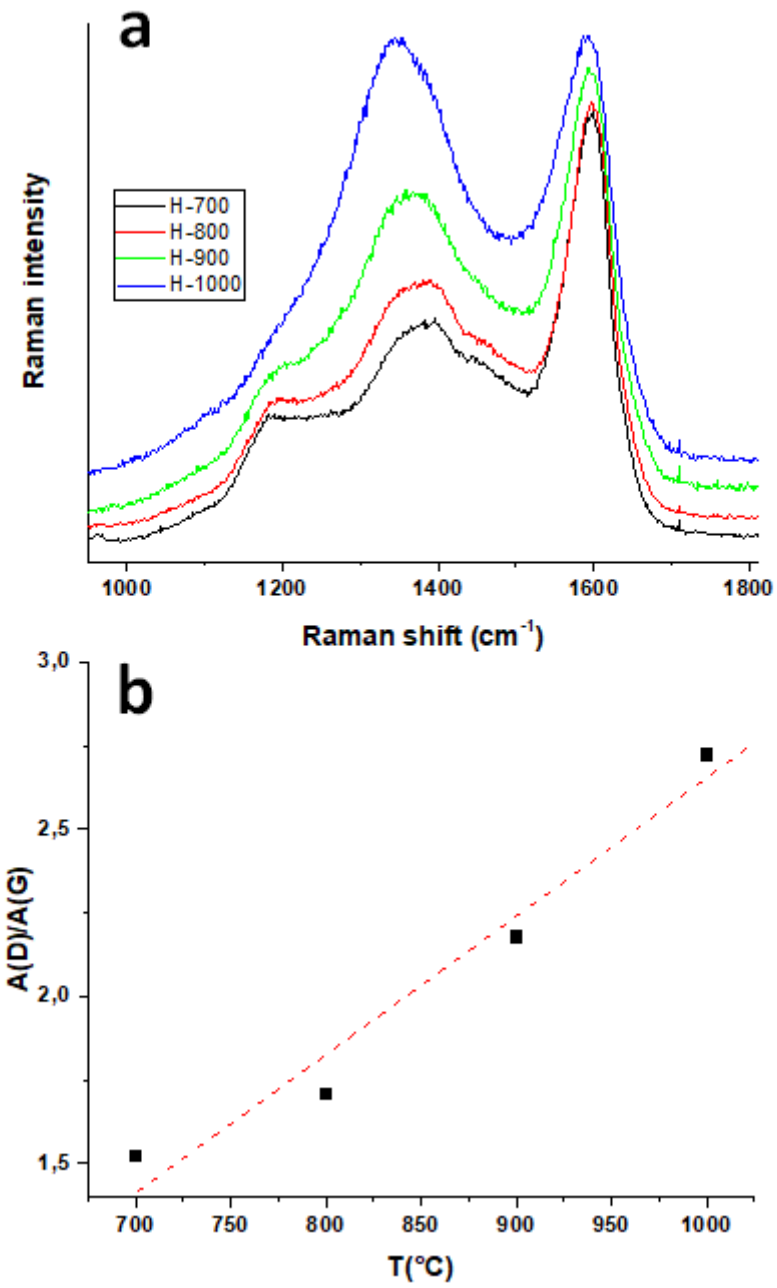
a
Raman intensity
H-700
H-800
H-900
H-1000
1000
1200
1400
1600
1800
Raman shift (cm-1)
b
A(D)/A(G)
3,0
2,5
2,0
1,5
700
750
800
850
900
950
1000
T(°C)

Figure 9

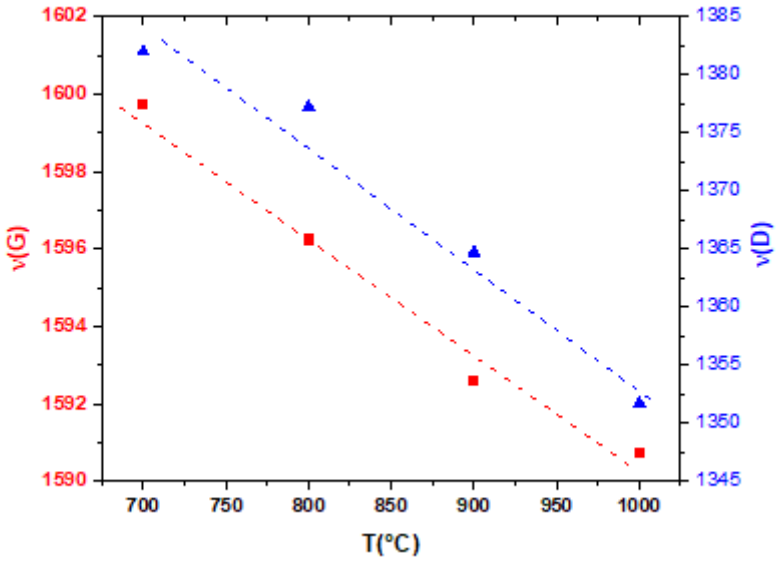
1602
1600
1598
1596
1594
1592
1590
ν(G)
1385
1380
1375
1370
1365
1360
1355
1350
1345
ν(D)
700
750
800
850
900
950
1000
T(°C)

Figure 10

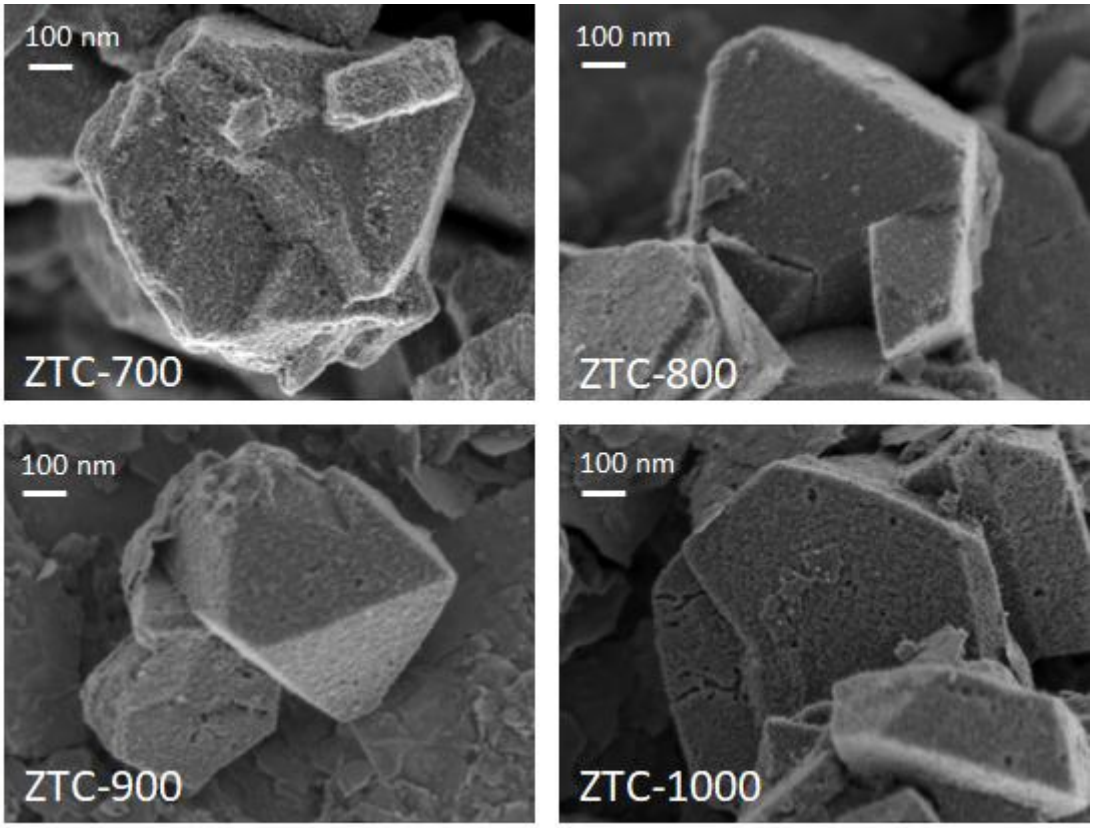

Figure 11

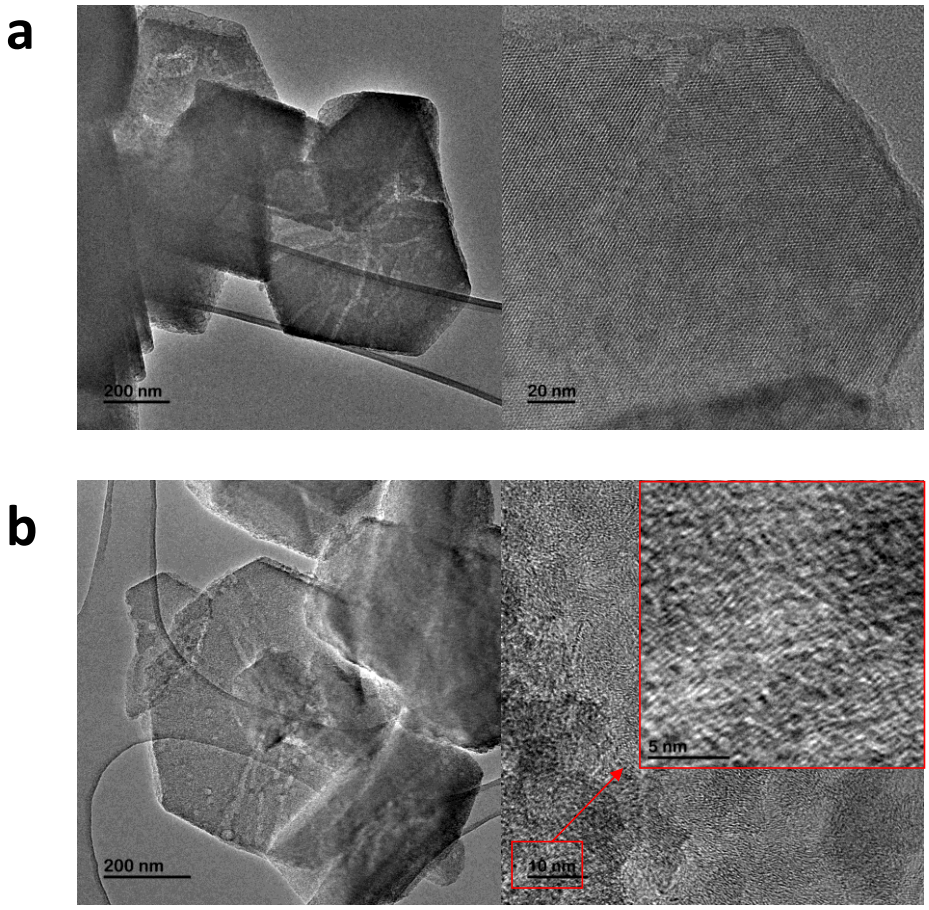

Figure 12

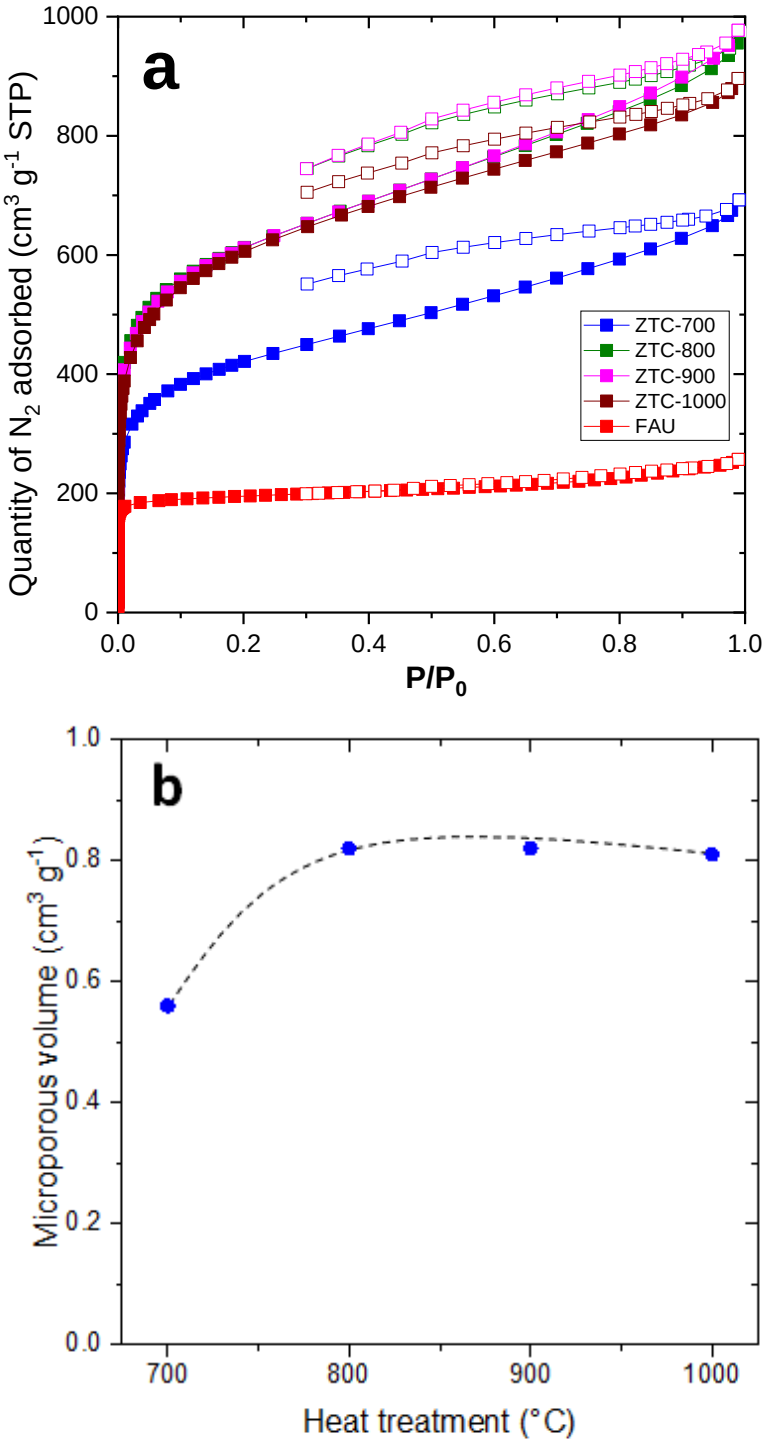
a
Quantity of N_2 adsorbed (cm^3 g^{-1} STP)
P/P_0
ZTC-700
ZTC-800
ZTC-900
ZTC-1000
FAU
b
Microporous volume (cm^3 g^{-1})
Heat treatment (°C)

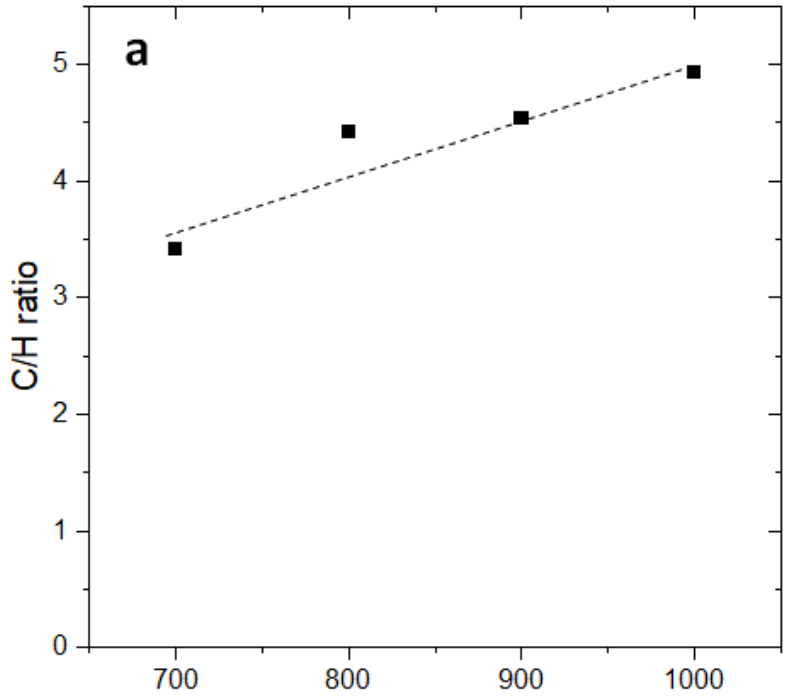
a
C/H ratio
0
1
2
3
4
5
700
800
900
1000

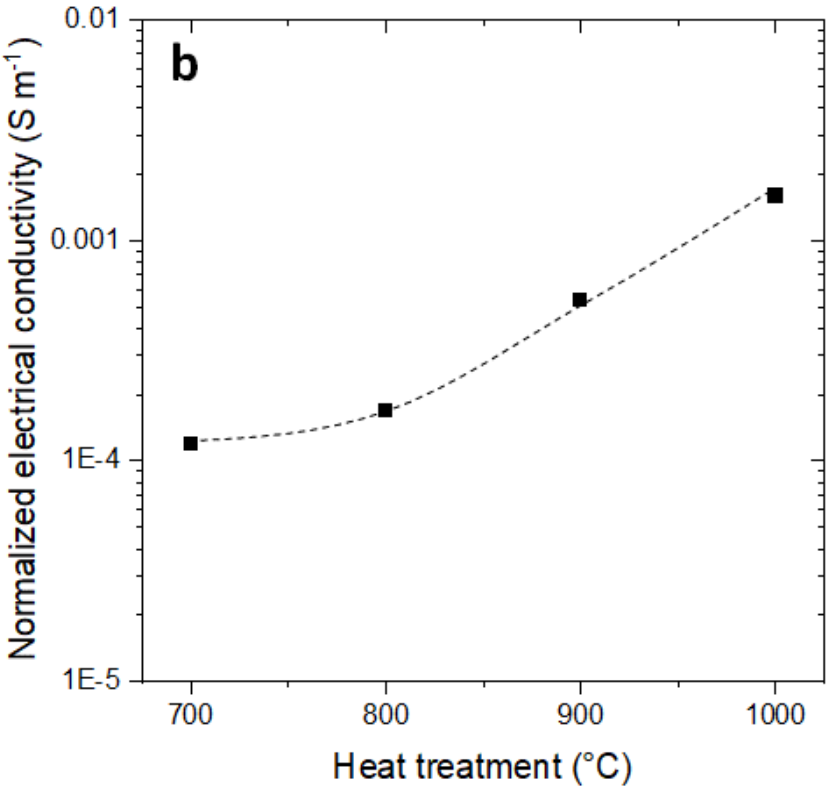
b
Normalized electrical conductivity (S m-1)
0.01
0.001
1E-4
1E-5
700
800
900
1000
Heat treatment (°C)

Figure 13

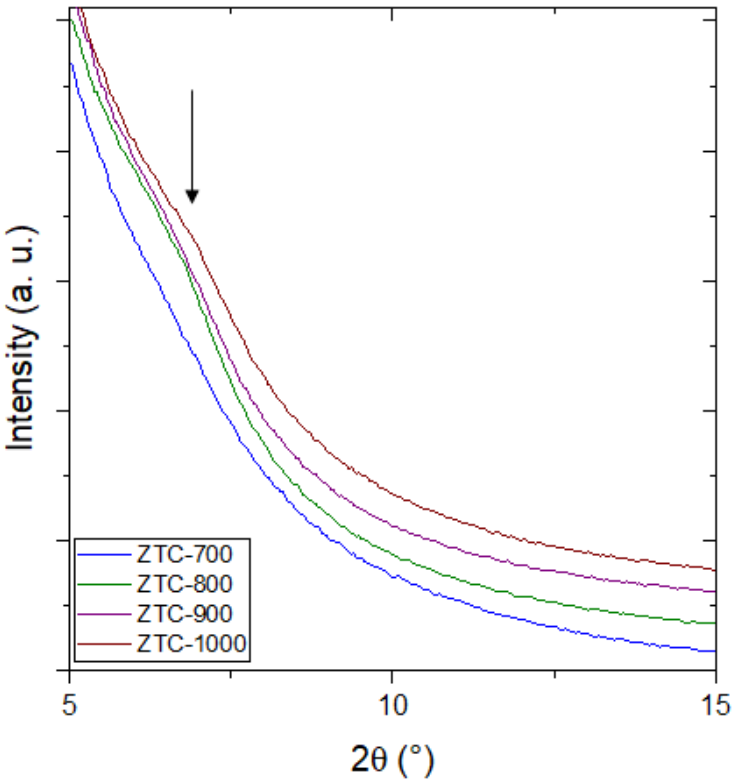

Graphical abstract